Journal of Applied Physics

# The structural and optical properties of black silicon by inductively coupled plasma reactive ion etching

Cite as: J. Appl. Phys. **116**, 173503 (2014); https://doi.org/10.1063/1.4900996
Submitted: 05 August 2014 • Accepted: 22 October 2014 • Published Online: 03 November 2014

**Martin Steglich, Thomas Käsebier, Matthias Zilk, et al.**







AIP Publishing

# The structural and optical properties of black silicon by inductively coupled plasma reactive ion etching

Martin Steglich,[a] Thomas Käsebier,[a] Matthias Zilk,[a] Thomas Pertsch, Ernst-Bernhard Kley, and Andreas Tünnermann
*Institute of Applied Physics, Abbe Center of Photonics, Friedrich Schiller University Jena, 07745 Jena, Germany*

(Received 5 August 2014; accepted 22 October 2014; published online 3 November 2014)

Black Silicon nanostructures are fabricated by Inductively Coupled Plasma Reactive Ion Etching (ICP-RIE) in a gas mixture of $SF_6$ and $O_2$ at non-cryogenic temperatures. The structure evolution and the dependency of final structure geometry on the main processing parameters gas composition and working pressure are investigated and explained comprehensively. The optical properties of the produced Black Silicon structures, a distinct antireflection and light trapping effect, are resolved by optical spectroscopy and conclusively illustrated by optical simulations of accurate models of the real nanostructures. By that the structure sidewall roughness is found to be critical for an elevated reflectance of Black Silicon resulting from non-optimized etching processes. By analysis of a multitude of structures fabricated under different conditions, approximate limits for the range of feasible nanostructure geometries are derived. Finally, the technological applicability of Black Silicon fabrication by ICP-RIE is discussed. 
[http://dx.doi.org/10.1063/1.4900996]

## I. INTRODUCTION

Silicon micro- and nanostructures have a broad, emerging application spectrum ranging from optics and optoelectronics over chemical and biological sensing to photo-electrochemical energy harvesting and energy storage. Besides the general feasibility of deterministic structures,[1,2] a vast number of different self-organized fabrication methods for silicon nanostructures have been developed over the past decades. Except for porous silicon obtained by electrochemical etching,[3,4] most of the produced structures exhibit tapered profiles that result in reduced interface reflection for incident light.[5,6] While structures fabricated by the vapor-liquid-solid (VLS) approach[7,8] or by wet-chemical catalytic etching[9–11] are usually called "silicon nanowires," structures obtained by repeated pulsed laser irradiation[12,13] or dry etching[14,15] are typically referred to as "Black Silicon." Comparing the different attempts of nanostructure formation, the last-mentioned dry etching method exhibits some distinct advantages. First, it is a reliable and reproducible, yet self-organized process that does not necessitate any additionally applied mask. Second, the method leaves crystallographic intact nanostructure surfaces free of chemical contaminations, in contrast, e.g., to structures obtained by VLS and wet-chemical etching or pulsed laser irradiation. Third, it cannot only be applied to poly- and monocrystalline wafers,[16] but also to amorphous or crystalline silicon thin films.[17] Lastly, the dry etching technique is capable of being integrated into in-line production facilities which is of great importance for high-throughput application fields like photovoltaics.

Historically, dry etching of Black Silicon has been known for decades as undesired byproduct of vertical silicon deep etching in $SF_6$-$O_2$ plasmas.[14] Due to the random formation of micromasks (mainly consisting of silicon oxyfluoride), "silicon grass" develops in the etched trenches during fabrication. Relying on this effect, Jansen *et al.* proposed the so-called "Black Silicon method" in 1995 as a tool to identify optimal conditions for vertical silicon deep etching in $SF_6$-$O_2$-$CHF_3$ mixtures.[14] Even before, Gittleman *et al.* from the RCA laboratories utilized dry etching in a chlorine plasma to produce non-reflecting Black Silicon surfaces for, e.g., improved absorbers for solar thermal energy conversion.[18] In 2001, Zaidi *et al.* published an extensive study on solar cells textured by reactive ion etching (RIE) in $SF_6$ and $O_2$, paying, however, little attention to the actual dry etching process.[19] During the last decade, only few publications treated Black Silicon formation by RIE in $SF_6$ and $O_2$. While Dussart's work examines Black Silicon etching at cryogenic temperatures,[15] Pezoldt *et al.* describe nanostructure fabrication at temperatures between 20 and 30 °C.[20] In addition, Jansen *et al.* studied the occurrence and the possible prevention of Black Silicon using different dry etching techniques.[21,22]

In order to close the experimental gap between the low and high temperature Black Silicon etching regimes, this paper summarizes our studies concerning Black Silicon fabrication by inductively coupled plasma (ICP-RIE) at moderate temperatures (−40 °C…−30 °C) that we conducted over the last years. Particularly, the dependencies of nanostructure morphology and optical properties on the important processing parameters (etch duration, gas composition and pressure) are investigated and explained comprehensively. In addition, an attempt is made to draw the big picture of Black Silicon processing using RIE by discussing our findings in the context of other authors' results.

[a]M. Steglich, T. Käsebier, and M. Zilk contributed equally to this work.

 

## II. EXPERIMENTAL

Black Silicon nanostructures were fabricated by dry etching in a SF6-O2 plasma using an SI-500 °C plasma reactor from Sentech Instruments. The reactor is equipped with a planar ICP source for the formation of high density plasmas. An additional RF source is coupled capacitively from the substrate holder and is used to adjust the substrate bias voltage. This allows tuning the energy of the ions that are accelerated towards the sample independently from the plasma density which is determined by the ICP power. The ICP power was fixed to 750 W in all processes discussed here. Nanostructure fabrication was carried out on 6 in. double-side polished, p-type silicon substrates with a thickness of 425 $\mu$m and a resistivity of 1–5 $\Omega$ cm. Substrate cooling was achieved by helium gas mediated thermal coupling to a heat sink that is continuously chilled by a refrigerated circulator. A vacuum sealing prevents the diffusion of He into the process chamber. The substrate temperature is assumed to correspond to the temperature of the heat sink that was monitored and controlled with a thermocouple. During the etching processes discussed in this paper, the measured temperature rises approximately linearly with etch time, starting from −40 °C, to −32 °C after 10 min. The etch durations were kept constant at 10 min, apart from the investigation of structure evolution where also shorter etch durations were used.

Optical spectra of the nanostructured silicon wafers were taken with a PerkinElmer Lambda 950 spectrometer equipped with an integrating sphere. Morphological structure properties were investigated with a scanning electron microscope, by taking both cross-section and top-view images of the samples, as well as illustrative images under an angle of 30°. To account for the statistical nature of the nanostructures properly, large field-of-view images were taken and analyzed statistically. Mean lateral structure dimensions were measured by means of calculating the minimum value of the two-dimensional, radial autocorrelation function of 25 $\times$ 25 $\mu$m$^2$ large top-view images. This value, which scales roughly with the mean etch pore diameter, will be utilized as characteristic *correlation length* $L_C$ in the following. The peak-to-valley depth $H$ of the structures was measured directly in cross-section images. Except from the wafer edge, where the substrate is mechanically clamped to the substrate holder, the fabricated Black Silicon structures are homogenous (or, more specifically, their statistical morphology parameters) over the whole 6 in. wafer.

To discuss the optical properties of the fabricated Black Silicon nanostructures, Finite-Difference Time-Domain (FDTD) simulations were performed with the open source software MEEP (Ref. 23) on virtual Black Silicon structures that emulated the experimentally observed structure parameters on an area of 5 $\times$ 5 $\mu$m$^2$. In the lateral directions periodic boundary conditions were assumed and along the propagation direction the computational domain was terminated by perfectly matched layers. The silicon substrate was assumed to be infinitely thick and reflections from the polished rear side were not taken into account. The whole structure was discretized with a spatial resolution of 7.5 nm.

## III. RESULTS AND DISCUSSION

### A. Structure evolution during etching

The evolution of Black Silicon nanostructure fabrication by ICP-RIE in a $SF_6$-$O_2$ plasma is studied at a fixed working pressure of 2 Pa at equal $SF_6$ and $O_2$ flows of 60 sccm. Figure 1 gives a comprehensive morphology overview (30° elevation, cross-section and top-view) of the structures evolving after 2 min, 3 min, 5 min, and 10 min. In the discussion of the evolution of the Black Silicon structures, we will rely on the extensive studies of $SF_6$-$O_2$ etching process by Dussart and co-workers[15,24–26] as well as the pioneering work of Jansen, de Boer and co-workers who first described the Black Silicon process.[14,27]

Generally two reactions occur in the presence of the $SF_6$-$O_2$ plasma. First, fluorine radicals F* etch the silicon surface chemically under the formation of volatile $SiF_4$

$$\mathrm{Si} + 4\mathrm{F}^* \rightarrow \mathrm{SiF}_4\uparrow . \tag{1}$$

Second, ionized etch products $SiF_y^+$ react with oxygen radicals O* and form a silicon oxyfluoride layer[14,24]

$$\mathrm{SiF}_y^+ + x\mathrm{O}^* \rightleftharpoons \mathrm{SiO}_x\mathrm{F}_y. \tag{2}$$

This layer protects the silicon surface from further chemical etching by fluorine radicals. However, the layer is not very stable and dissociates when heated[24] or under ion bombardment from the plasma.[25] Thus, the actual formation of a passivation layer is strongly influenced by the substrate temperature, the ion energy (i.e., the substrate self-bias) and the oxygen flow.

For anisotropic etching in microfabrication usually some substrate self-bias is set so that the impinging ions are strongly directional. The oxygen flow is then adjusted to enable the formation of a passivation layer on vertical faces on which the energy transfer of the impinging ions is low due to the grazing incidence. At the same time, the formation of a stable passivation layer on the horizontal faces is inhibited due to the stronger ion bombardment. Increasing the oxygen flow over a certain threshold leads to a stronger passivation that also inhibits the etching on horizontal faces and causes a sharp drop of the etch rate.[25,27] This so-called overpassivating regime leads to the formation of Black Silicon structures.[15] Apparently, in the initial stage of structure formation, the substrate roughness is strongly increased (compare images after 0 min and 0.5 min in Figure 1). Afterwards, this roughness becomes more and more pronounced due to the trenching effect:[28] As impinging ions are (partially) reflected at the sloped sidewalls of the nano-roughness, enhanced physical etching occurs in its valleys (as compared to the roughness peaks, see image after 1 min). In turn, the passivating $SiO_xF_y$ layer is removed faster in the valleys. Finally, at some point the $SiO_xF_y$ passivation layer will be removed completely in the roughness's deepest valleys. Now, the spontaneous formation of isolated etch pits can be observed as the underlying pure silicon is rapidly etched by fluorine radicals F*. This situation is shown in the SEM images in Figure 1 that were taken after an etch duration of 1.5 min.

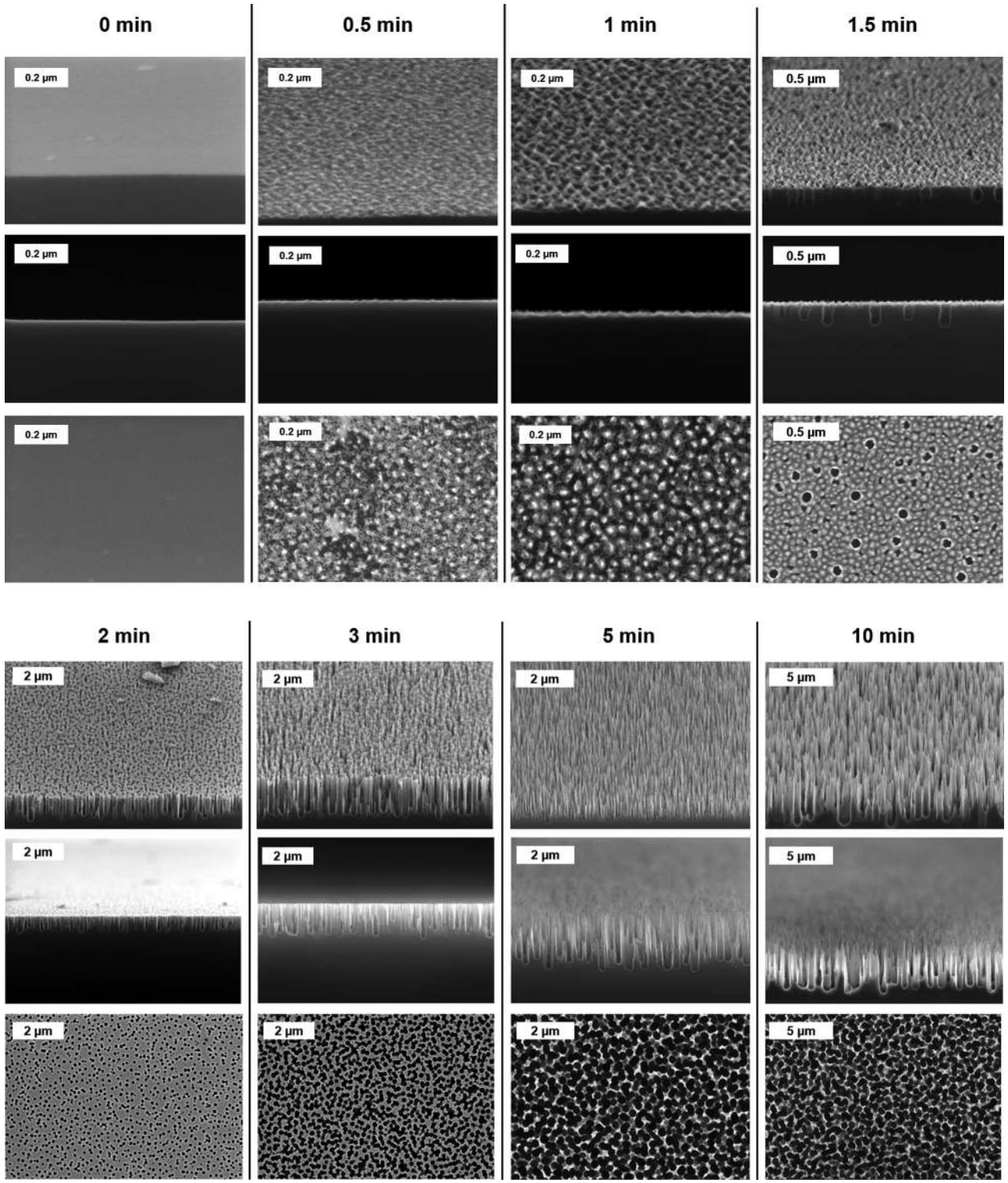


FIG. 1. Structural evolution of Black Silicon by ICP-RIE, inspected after 0.5 min, 1 min, 1.5 min, 2 min, 3 min, 5 min, and 10 min. The upper row displays tilted SEM images, the middle and the lower row display cross-section and top-view images, respectively. Attention should be paid for the different scale bars.

Once etch pits have formed, etching proceeds anisotropically as the ion bombardment inhibits the passivation layer formation on the horizontal etch pit ground much stronger than on the vertical sidewalls. Also, the exothermic nature of the fluorine etching reaction might contribute to weakening the passivation layer formation at the pore ground by local heating of the substrate.[25,26] Thus, in the course of further etching, the initial vertical pores quickly become deeper, but also wider, as the etching is not stopped completely at the sidewalls (images after 2 min). Eventually, the pores intersect and become more and more connected to each other (images after 3 min). At the same time, new shallow pores can develop in the open space between the already existing, older pores. After 5 min, both of these processes have continued long enough to yield a complete pore interconnection all over the sample surface. The result is a first

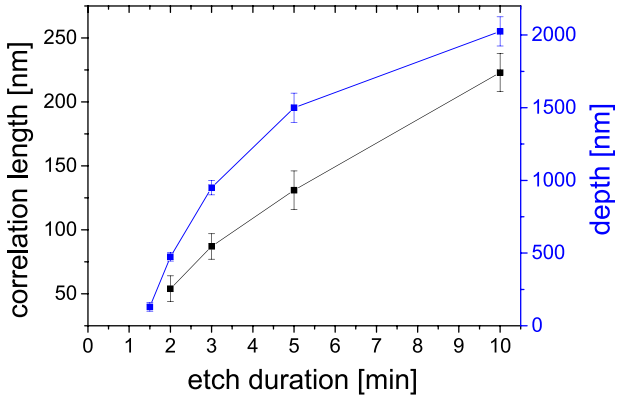


FIG. 2. Morphological parameters (lateral correlation length $L_C$ and structure depth $H$) as a function of etch duration. First Black Silicon nanostructures with sharp structure features appear after 5 min.

true "Black Silicon" nanostructure, consisting of silicon needles that evolve at the cutting sites of the interconnecting pores. Afterwards, further etching increases both the mean pore diameter and depth while the principle appearance of the nanostructure remains like before (see images after 10 min of etching).

Figure 2 displays the dependency of the morphological parameters correlation length and structure depth on etch duration. As discussed before, it can be seen clearly that both parameters increase with etch duration. At 5 min, when the correlation length approaches the mean pore separation, Black Silicon nanostructures with sharp tips develop due to the overlap of pores with positively sloped sidewalls. Then, longer etching leads to the development of structures with higher correlation lengths and depths, where the related parameter ratio stays nearly constant.

Open questions related to the evolution of Black Silicon by ICP-RIE concern the still unexplained initial roughness formation that takes place during the first minute after process start. Two underlying mechanisms seem to be plausible. First, the roughness might simply arise from the shot-noise-like, infrequent sputtering of the sample surface by plasma ions.[29,30] Second, $SiO_xF_y$ nanoparticles might form in the plasma and precipitate on the sample surface, yielding a random mask for the initial physical etching and, thus, a strongly increased surface roughness.[22] However, further experimental evidence is necessitated to resolve the issue of nanostructure initiation conclusively.

The most intriguing feature of ICP-RIE processed Black Silicon is its strong antireflection effect for incident light throughout the whole spectral region from the ultraviolet to the near-infrared, giving this nanostructure its very appropriate name. Figure 3 shows hemispherical reflectance and absorptance spectra around 1100 nm (i.e., close to the silicon bandgap) of the samples etched for different durations. For comparison, also the spectra of a polished silicon substrate before etching are displayed as reference.

As can be seen from the reflectance spectra, even right after the onset of structure formation after 2 min, the optical reflectance at the air-silicon interface is significantly reduced and further decreases in the following course of pore growth and deepening (3 min). Beginning from the point of sharp tip formation after 5 min, the reflectance is nearly completely suppressed and *Black* Silicon formation is complete. The absorptance spectra on the right side of Figure 3 show that the emerging Black Silicon structures also give rise to a pronounced light trapping effect that significantly increases the absorption in the vicinity of the silicon band gap. The possible nature of the anti-reflection and light trapping effects will be discussed further below.

### B. Influence of the process gas composition $O_2$:$SF_6$

In Sec. III A, all discussed nanostructures have been obtained using equal flows of 60 sccm for the etch gases $O_2$ and $SF_6$. However, the strong influence of silicon oxyfluoride passivation during structure evolution suggests that the gas composition has a major influence on the resulting Black Silicon morphology. For this reason, experiments were conducted with varying gas compositions at process conditions like before and a constant etch duration of 10 min. Figure 4 shows SEM images of structures produced with 80 sccm $O_2$ and 60 sccm $SF_6$, 60 sccm $O_2$ and 60 sccm $SF_6$, 60 sccm $O_2$ and 90 sccm $SF_6$, as well as 60 sccm $O_2$ and 129 sccm $SF_6$. As can be seen from these images, the structure sidewalls tend to become more and more frayed with increasing $SF_6$ content in the etching plasma. This trend is attributed to the formation of shallow nanopores at the structure sidewalls, which are clearly visible in the SEM image of the structures with the highest $SF_6$ flow. On the other hand, a high $O_2$ content leads to very smooth structure sidewalls. Furthermore, a quantitative analysis of the morphological structure parameters, displayed in Figure 5, reveals a decreasing correlation length $L_C$ and structure depth with increasing $O_2$ content. This behavior arises from the complex interaction of the etch species $O_2$ and $SF_6$ in the plasma. While $O_2$ is important for the passivation reaction according to Eq. (2), $SF_6$ yields the

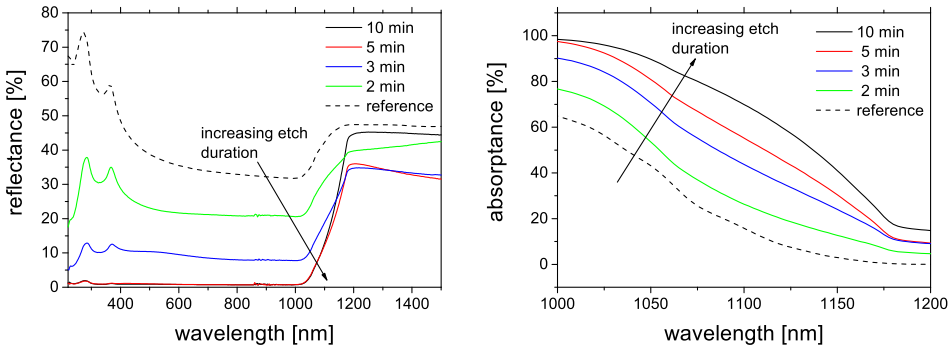


FIG. 3. Evolution of reflectance (le.) and absorptance around 1100 nm (ri.) during Black Silicon etching by ICP-RIE. Spectra of a polished silicon wafer are shown for reference.

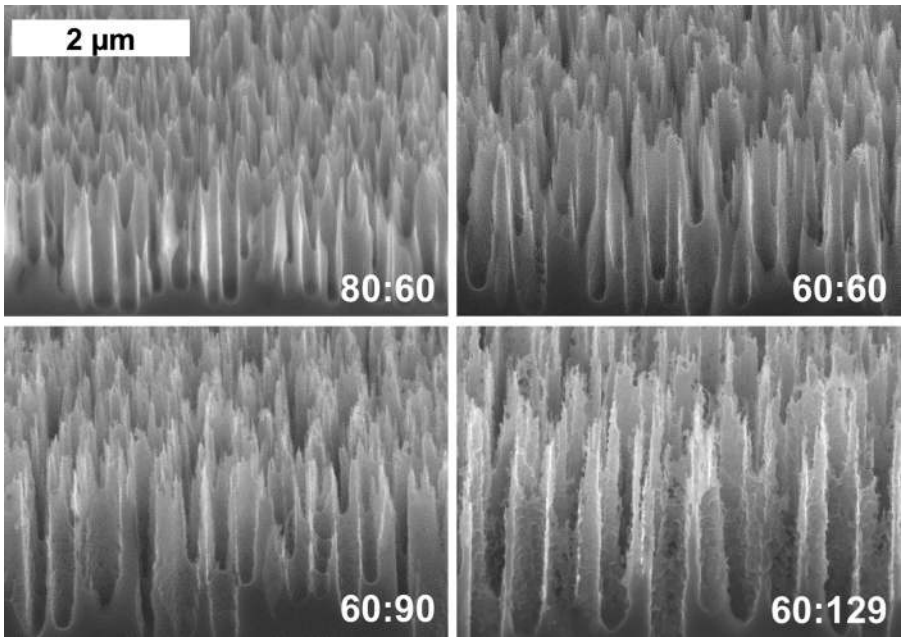


FIG. 4. SEM images of Black Silicon fabricated under different gas flow ratios of $O_2$ and $SF_6$ (flows are given in sccm).

actual etching component F* upon dissociation for the etching reaction (Eq. (1)). Thus, a high $O_2$ content results in a high passivation component in the plasma that hinders the silicon etching reaction.[31] As a consequence, both $L_C$ and structure depth are lowered in high oxygen plasmas. Otherwise, high $SF_6$ plasmas possess a high etching capability and hence provide Black Silicon nanostructures with raised geometrical dimensions and, eventually, even give rise to frayed structures due to undesired sidewall pore etching.

The variation of gas composition also has a strong impact on the optical behavior of produced nanostructures. Figure 6 displays the reflectance spectra of the samples produced with different gas compositions. The reflectance is seen to be exceptionally low (around 1%) in the case of equal gas flows of $O_2$ and $SF_6$ and, also, for fabrication in the oxygen-richer plasma with 80 sccm $O_2$ flow. A higher $SF_6$ content during structure processing, however, has an increasingly detrimental effect on the AR effect of the produced nanostructures. In fact, a distinct bump in the visual spectral range can be observed in the reflectance spectra of samples obtained in $SF_6$ rich plasmas. Despite the strong effect of gas composition on the reflectance in the visible spectral range, the light trapping properties in the near-infrared are only weakly affected by the additional sidewall roughness that is induced by high $SF_6$ flows (not shown here).

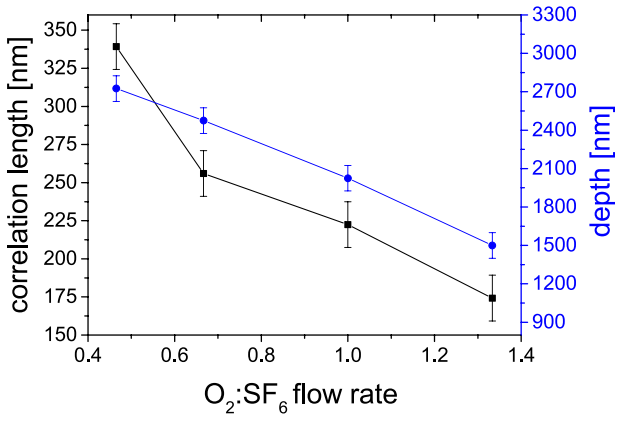


FIG. 5. Morphological parameters of Black Silicon nanostructures obtained with varying gas composition in the plasma.

### C. Dependence on process pressure

Another important parameter during Black Silicon fabrication by ICP-RIE is the process pressure. Since it allows control over the energy and directionality of the impinging ions, it has presumably also a considerable impact on the resulting nanostructure morphology. Figure 7 shows Black Silicon nanostructures obtained under different process pressures at equal gas flows of 60 sccm each, after a fixed etch duration of 10 min. While the structures fabricated at lower pressures of 1 Pa and 2 Pa look quite similar at first glance, structures at higher pressures of 3 Pa and 4 Pa appear

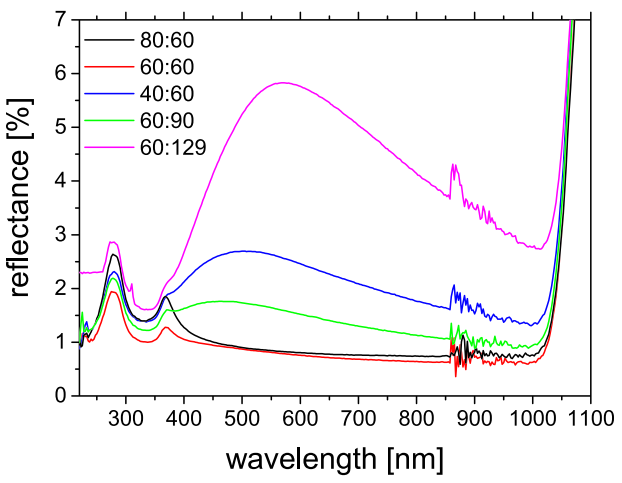


FIG. 6. Hemispherical reflectance spectra of Black Silicon nanostructured wafers, obtained under varying etch gas compositions $O_2$:$SF_6$. Flows are given in sccm in the legend.

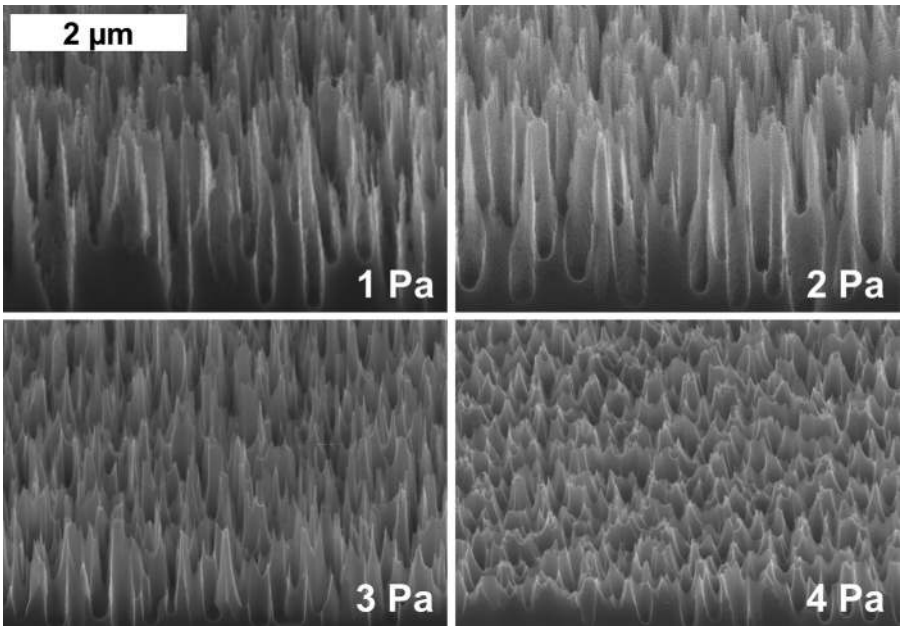


FIG. 7. SEM images of Black Silicon fabricated under different pressures.

strongly different. Besides their decreased structure depth, they furthermore exhibit less steep sidewalls. Both effects, the minor depth and the evolution of clearly positive sidewalls, are enhanced under pressure increase from 3 Pa to 4 Pa. The quantitative inspection of the morphological parameters by statistical analysis in Figure 8 clearly confirms the visual observation of decreasing structure depths for pressures greater than 2 Pa. In addition, also a continuous decline of the structure correlation length over the whole investigated pressure range is determined. As stated before, these changes in morphology under process pressure variation can be attributed to the varied influence of physical etching. If the pressure increases, the mean free path of the ions that are accelerated towards the sample decreases and, consequently, the highly anisotropic physical etching mechanism by ion bombardment is suppressed. Then, etching is less directional and rather isotropic etch profiles with positive sidewalls occur. As inevitable side effects of the more isotropic etch process, the final structures are less deep and the correlation length is smaller since the smaller etch pores are less frequently consumed by the larger pores during structure evolution.

Like before, each sample from the process pressure variation shows a distinct AR effect for incident light (Figure 9). While the reflectance of the samples obtained under 2 Pa and 3 Pa exhibit a considerably low reflectance of about 1% in the Vis, the samples fabricated under high (4 Pa) and low pressure (1 Pa) show a significantly raised reflectance of about 3% and 1.7%, respectively. Here, the relatively high reflectance of the high pressure sample can be attributed to the sample's insufficiently low structure depth of only 600 nm. Nevertheless, it should be noted that the value of 3% is, still, an exceptionally low degree of reflectance for a high index silicon surface.

### D. Discussion of optical properties

In the following we will discuss the origin of the observed optical properties, namely, the low reflectance and the near infrared light trapping, and the influence of the geometrical parameters onto these.

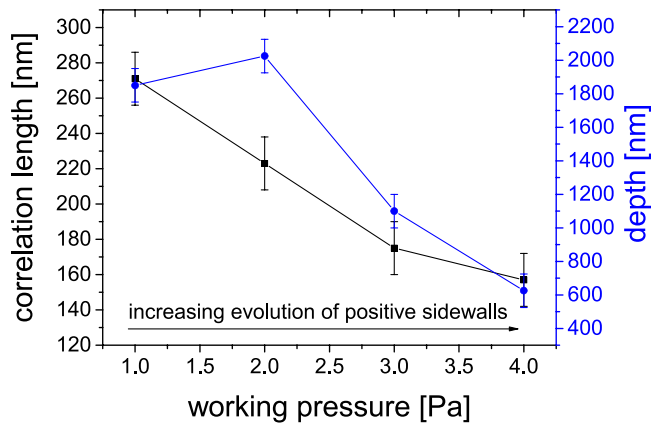


FIG. 8. Morphological parameters (correlation length $L_C$ and structure depth $H$) of Black Silicon fabricated in different process pressures.

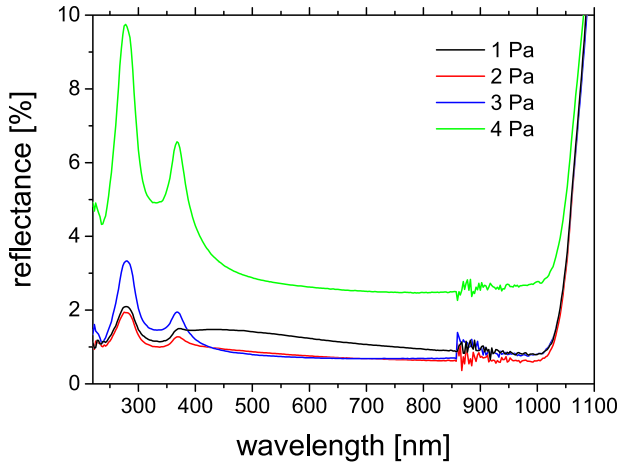


FIG. 9. Hemispherical reflectance spectra of Black Silicon nanostructured wafers, obtained under different process pressures.

Usually the anti-reflection properties of structured interfaces are explained in terms of one of two limiting cases: Effective medium theory[32] or geometrical optics.[33,34] Effective medium theory is applicable when the correlation length $L_c$ is much smaller than the scaled wavelength $\lambda/n_{Si}$ (whereby $n_{Si}$ is the silicon refractive index). In this case no structural features are resolved by the incoming wave and a depth dependent average refractive index can be assigned to the structure by applying some mixing formula (e.g., Ref. 35). Then, the anti-reflection properties can be explained in terms of a gradient index effect.[32] Geometrical optics applies when correlation length $L_c$ is much larger than the wavelength $\lambda$ and diffraction effects can be neglected. In this case the incoming light can be described by a bundle of rays and the anti-reflection properties of a structured interface can be explained in terms of the average number of reflections a ray experience before it is finally lost.

However, most Black Silicon structures exhibit a correlation length in the order of the scaled wavelength ($L_c \sim \lambda/n_{Si}$). Thus, neither of the aforementioned limiting cases is met exactly. This does not mean that the approximate descriptions fail completely and they might still yield reasonable qualitative descriptions of the optical properties of the structures. Yet they are not able to provide reliable quantitative figures on the typical scales of the Black Silicon structures. To obtain those, a wave optical description of the light propagation inside the structure is required. The presence of the near infrared light trapping indicates that some scattering into large angles occurs in the infrared and, thus, even stronger scattering can be expected at smaller wavelengths in the visible and ultraviolet. Under those circumstances, it has to be expected that even scalar description of the optical waves is not accurate enough and a fully vectorial wave-optical method has to be used to describe the light interaction with the Black Silicon structures correctly. We therefore decided to conduct large scale FDTD simulations to gain further insight into the light propagation inside the fabricated structures.

For this purpose, we created a numerical model of a typical Black Silicon structure by extracting the positions and shapes of the etch pits from a top-view SEM image as shown in Figure 1 and removing the according volume from a voxel representation of the silicon substrate. A part of the resulting structure is shown in Figure 10(a). This basic structure has a correlation length $L_C$ of 207 nm and a peak to valley height $H$ of 1.75 $\mu$m. The influence of the geometric parameters

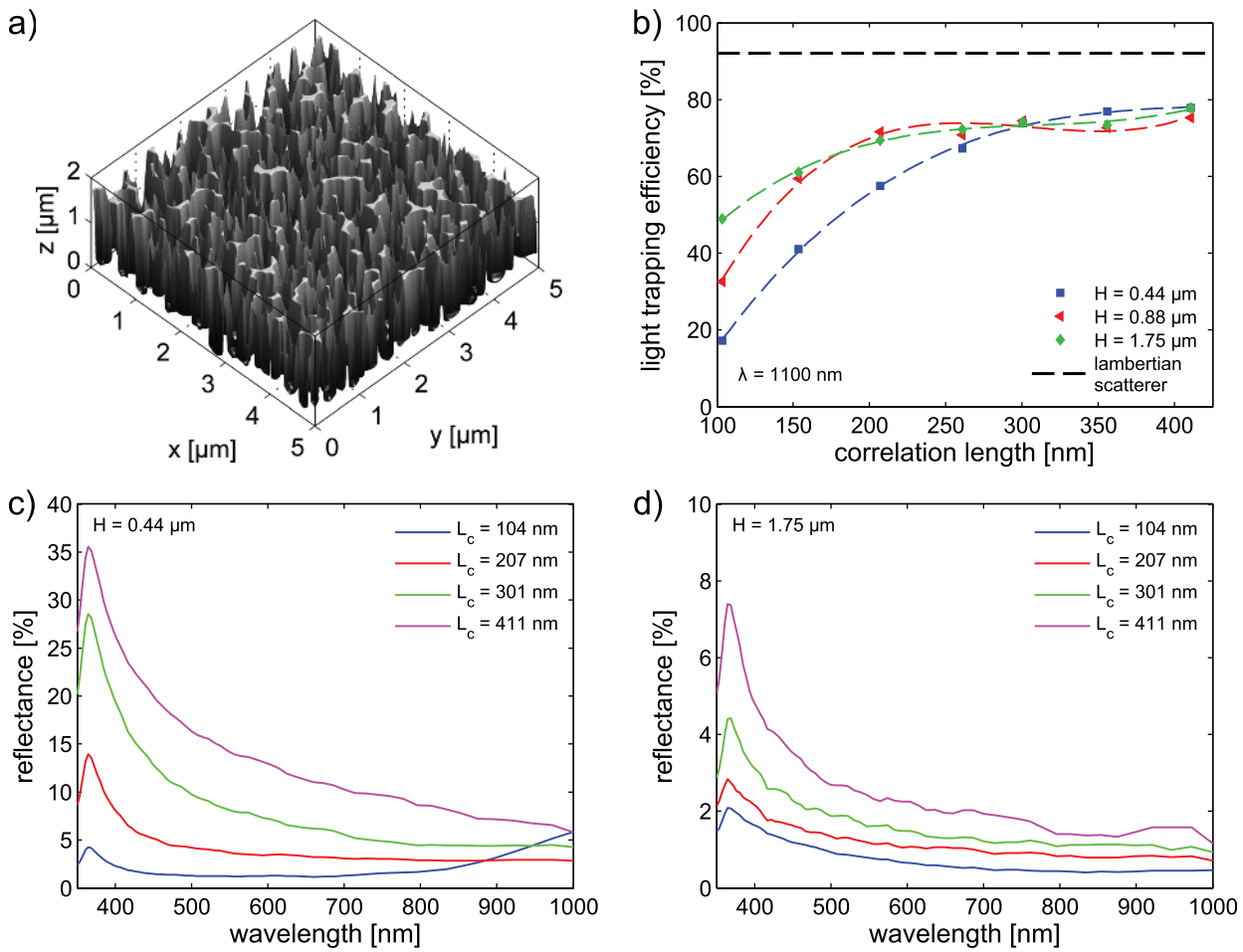


FIG. 10. Optical properties of various Black Silicon geometries simulated with the FDTD method: (a) basic structure that was modified by lateral and vertical scaling to obtain Black Silicon with different structural parameters, (b) light trapping efficiency of the simulated structures at a wavelength of $\lambda = 1100$ nm in dependence of the correlation length $L_C$, (c) reflectance spectra for various correlation lengths at a fixed structure depth $H$ of 0.44 $\mu$m, and (d) the same for a structure depth $H$ of 1.75 $\mu$m.

was studied by scaling the basic structure laterally and vertically to produce different structure depths and correlation lengths.

To quantify the impact of the structural variations on the light trapping properties of the simulated geometries, we define a light trapping efficiency $\eta_{LT}$ as the fraction of the transmitted power that is scattered out of the loss cone of total internal reflection. The value of the light trapping efficiency can be calculated by summing the transmittance of all scattered waves $T(k_x, k_y)$ whose transverse wave vector $(k_x, k_y)$ exceeds the free space wave number $k_0 = 2\pi/\lambda$ of the incident light

$$\eta_{LT} = \frac{1}{T_{tot}} \sum_{k_x^2+k_y^2>k_0^2} T(k_x, k_y). \quad (3)$$

This corresponds to the fraction of light that experiences total internal reflection at the polished rear side of the wafer. The light trapping efficiency is normalized to the total hemispherical transmittance $T_{tot}$ to eliminate the influence of a varying reflectance. Of course, this definition does not include all factors that might be important for light trapping. For example, the angle dependent internal reflectance of the Black Silicon surface is completely ignored. Nevertheless, this definition is reasonable as it quantifies at least the fraction of light that might experience multiple bounces inside the silicon substrate before being coupled out again due to scattering. Furthermore, the numerical value of $\eta_{LT}$ can be calculated with reasonable effort from a single FDTD simulation.

The influence of correlation length and structure depth onto the light trapping efficiency is shown in Figure 10(b) along with the limit of a Lambertian scattering surface for Ref. 36. It can be seen that the light trapping efficiency generally tends to increase with correlation length whereby the impact is strongest when the structure depth is low. At low correlation lengths an increased structure depth also improves the light trapping. However, at larger correlation lengths it seems to approach a common value regardless of the depth. We would like to point out that the trend in the light trapping efficiency predicted by the simulations is consistent with the experimental results that were obtained upon varying the etch time: With increasing etch time, both the structure depth and correlation length increase. At the same time the near infrared light trapping in the near infrared gets more pronounced as shown on the right of Figure 3.

Qualitatively, the influence of the geometrical parameters can be understood by considering that the coupling into different scattering angles is mediated by the spatial frequency components of the lateral material distribution of the Black Silicon structures.[37] A low correlation length corresponds to a material distribution that predominantly contains high spatial frequencies. Those high frequencies would couple the incident light to evanescent waves that do not propagate while lower spatial frequency components that could excite propagating waves are comparably weak. On the other hand, a larger correlation length corresponds to a narrower spatial frequency distribution and, consequently, a stronger coupling to propagating waves. In this case, scattered waves will also be coupled back to low propagation angles with increasing propagation length and some equilibrium will form where the width of the scattering distribution saturates. According to this reasoning, it is to be expected that even larger correlation lengths will finally cause a decline of the light trapping as the spatial frequency spectrum of the permittivity distribution will get too narrow to excite large scattering angles.

Reflectance spectra of the simulated Black Silicon structures are shown in Figures 10(c) and 10(d) for various correlation lengths and two structure depths. Generally, the reflectance increases with the correlation length and strongly decreases with the structure depth (note the different scales in the figures). To explain this behavior in terms of the qualitative discussion from above one could argue that larger structures exhibit more low spatial frequency components that couple the incident light to propagating backscattered waves. Or, to put it into a simplified frame: Larger structure faces with low inclination, e.g., pore grounds or larger needle tips, are better "resolved" by the incident wave and, thus, reflect more light. Fortunately, as long as the transition from the air region to the silicon substrate is sufficiently deep, i.e., the structures are deep enough and exhibit steep sidewalls, the fraction of backscattering is low, albeit not as low as for a true gradient index layer that can achieve virtually zero reflectance.[32,38]

A notable exception to these general trends can be seen for the lowest correlation length and structure height of only 0.44 $\mu$m in Figure 10(c). Here, the reflectance clearly exceeds those of larger structures above $\lambda = 900$ nm. At those large wavelengths, the smallest structure most likely approaches the effective medium limit of a true gradient index structure. However, it has been shown in the literature that a gradient index layer fails when its thickness is less than about half of the wavelength of the incident light.[39] Interestingly, larger structures that are not effective medium like are less prone to such a reflectance increase at low structure depths. A similar behavior was observed by Boden and Bagnall who studied periodic silicon antireflection structures with feature sizes in the order of the scaled wavelength.[6] To support this finding, the calculated relationship between reflectance and correlation length for the 0.44 $\mu$m deep Black Silicon structure is plotted in Figure 11 for a fixed wavelength of $\lambda = 1100$ nm. It shows that there is indeed an optimum correlation length of about 200 nm, i.e., in a regime where the structure cannot be considered as an effective medium, where the reflectance is lowest.

Overall the simulated reflectance spectra resemble the experimentally observed behavior with one notable exception: The simulations discussed so far do not reproduce the reflection peak in the visible that appears upon the variation of etch gas composition (Figure 6). Besides the change of correlation length and structure depth, the most striking feature of those structures is the obvious change in the sidewall roughness of the silicon needles (Figure 4). We therefore tried to incorporate this roughness into our simulated Black Silicon structure by introducing spherical voids at about 1.25% of all surface voxels (being defined as voxels having less than 17 neighbors). The evolution of the synthetic Black

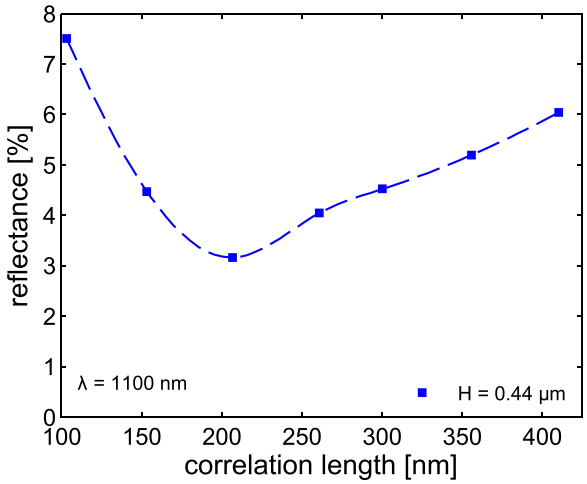


FIG. 11. Simulated hemispherical reflectance at $\lambda = 1100$ nm in dependence on the correlation length.

Silicon model with increasing radii of the added defects is displayed on the left side of Figure 12. The right side of Figure 12 shows that this modification indeed results in reflectance spectra that reproduce the experimentally observed behavior very closely. Hence, it can be concluded that the reflectance increase in the visible spectral range as shown in Figure 6 is solely a result of the surface roughness induced by a raised $SF_6$ content in the etch gas. It can be speculated that this effect is most likely caused by resonant scattering at individual defects sites. Finally, it should be pointed out that the influence of the roughness diminishes towards the infrared and hence there is almost no effect on the light trapping properties of Black Silicon, neither in the simulated light trapping efficiency nor in the experimentally observed absorptance spectra (not shown here).

## IV. CONCLUSIONS

Black Silicon nanostructures possess potential to optically enhance various silicon-based optoelectronic devices like pin photodiodes, photoconductors and CMOS imagers,[40–42] as well as wafer-based and thin film silicon solar cells.[11,17,19,43–46] In addition, also pure optical applications like silicon lenses or windows for the IR and light absorbers[47] can greatly benefit from the exceptionally good antireflection effect induced by the needle-like Black Silicon nanostructure. Among the multitude of fabrication methods for Black Silicon, ICP-RIE seems to be the most reasonable choice for most of the named applications because of its very good repeatability and reliability, the excellent chemical and structural intactness of the produced structures,[20,48] and its applicability to all forms of silicon, irrespective of the degree of structural order.[16] However, different applications make different demands on the morphology of suitable Black Silicon nanostructures which can be hard to meet. For example, imaging devices are required to be image preserving, thus forbidding the utilization of strongly forward scattering Black Silicon structures for such applications. On the contrary, non-imaging optoelectronic devices like pin photodiodes or solar cells can take considerable advantage of light scattering into higher propagation angles in the absorber due to the light path enhancement at a fixed absorber thickness. While structures with strong light scattering abilities can be readily accomplished since the necessitated high correlation lengths ($L_C > 250$ nm) are realized easily by adjusting several ICP-RIE parameters, so far there is a certain lack of suitable, non-scattering Black Silicon structures with low correlation lengths. Figure 13 illustrates this issue in form of a morphology map by displaying the correlation length of fabricated Black Silicon nanostructures over their respective structure depth. The red line, representing a fit through all final Black Silicon structures, visualizes the rough trend of correlation lengths simultaneously increasing with structure depths, which has also been reported recently by Pezoldt *et al.*[20] The interdependency of correlation length and depth is caused by the fact that both pore widening and deepening in the course of structure evolution are similarly triggered by the ratio of the plasma's etching over passivation component. Thus, using ICP-RIE at non-cryogenic temperatures, we have not been

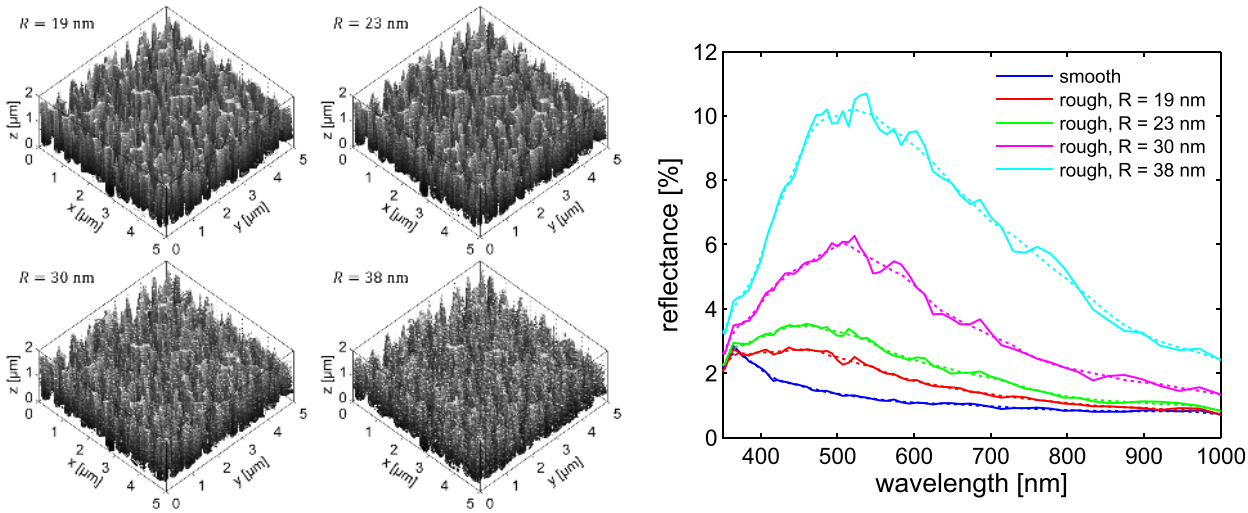


FIG. 12. Influence of the surface roughness on the reflectance of black silicon. On the left the analyzed geometry with various degrees of roughness (expressed in terms of the radius $R$ of the added surface defects) is shown. On the right the resulting reflectance spectra simulated with the FDTD method are plotted. The dotted lines show the average over the residual interference effects due the finite computational domain and serve as guides to the eye.

able to produce structures of low correlation length and high depth so far, i.e., moving further to the lower right corner of the morphology map in Figure 13. It might be possible that etching at deeper, cryogenic temperatures (lower than −100 °C) could be a solution to that problem, since the substrate temperature is known to be a critical parameter for the formation and stability of $SiO_xF_y$ passivation layers.[31,49] Although recently published work in the cryogenic etch regime did not yield nanostructures with shorter correlation lengths than in this work, further optimization of process parameters in this regime could successfully close the gap to structures with higher aspect ratios at low correlation lengths.[15]

In general, Black Silicon fabrication via reactive ion etching has proven to be astonishingly robust regarding substrate temperature variation. Besides successful structure formation at very low temperatures,[15,50] fabrication is generally possible at least up to 30 °C,[16,20,51] making the technique easier applicable for high-throughput production of, e.g., solar cells. Under constant etching conditions, the main drawback of substrate temperature increase is a gradual loss of sidewall passivation, leading to a slightly shallower structure with clearly porous sidewalls and a higher correlation length of 310 nm at 20 °C versus 216 nm at −38 °C (see Figure 14). Consequently, the raised correlation length together with the sidewall roughness causes an increased hemispherical reflectance of about 2% to 3%. To accommodate for this effect, the etching recipe should be adapted to strengthen the plasma's passivation capability; e.g., by increasing the $O_2$:$SF_6$ ratio.

An important feature of Black Silicon obtained by ICP-RIE is its excellent integrability into persistent CMOS manufacturing chains. Common masking materials like $SiO_2$ and photoresists can be used to fabricate the nanostructure precisely in defined areas. Exemplary, a $SiO_2$ thickness of 750 nm and resist thicknesses of few $\mu$m were found to be sufficiently thick for masking of Black Silicon fabricated under our standard conditions.

Another equally inevitable property of the structures discussed here concerns surface passivation which is of major importance for optoelectronic applications. Silicon nanostructures like Black Silicon, porous Silicon[52] or silicon nanowires[53,54] are often believed to inhibit improved optoelectronic devices due to drastically increased surface recombination of photogenerated carriers, despite the structures' beneficial impact on the optical absorption characteristics. First, this argument stems from the obvious fact that any nanostructure increases the surface area and, thus, the surface recombination. Second, chemical contaminations or structural defects introduced by the nanostructure fabrication method are often identified as cause for increased surface defect densities and the related increased surface recombination velocity. However, within this context considerable progress has been achieved recently. Applying ultra-thin, conformal $Al_2O_3$ coatings by Atomic Layer Deposition to samples from our lab, Otto *et al.* demonstrated a low temperature passivation scheme for Black Silicon resulting in remarkable effective carrier lifetimes of more than 1 ms.[55] Here, both the high chemical purity, as well as the structural integrity of the nanostructure surface of Black Silicon by ICP-RIE, has been identified as essential criteria for the obtained low surface recombination velocity. Interestingly, the thin (about 30 nm) conformal $Al_2O_3$ layers can even further reduce the already very low Black Silicon surface reflection in the UV region.[47] It should be noted that good surface passivation by thin, thermally grown $SiO_2$ is reported in the literature, too.[44] Altogether, it can be concluded that sufficient surface passivation of Black Silicon nanostructures by ICP-RIE is technologically feasible nowadays.

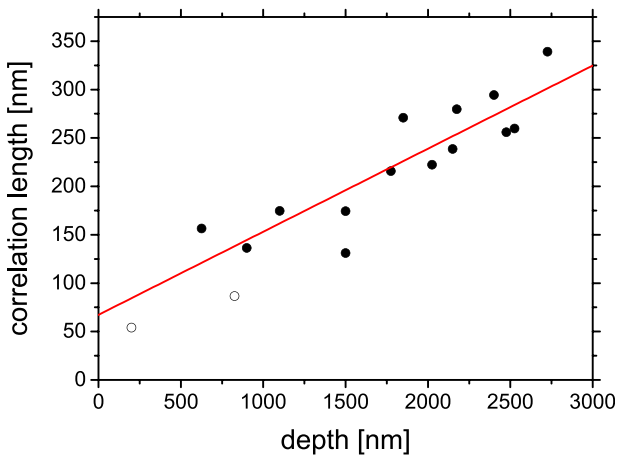


FIG. 13. Structure morphology map of Black Silicon fabricated by ICP-RIE at non-cryogenic temperatures. Open circles represent premature structures from the initial phases of structure formation. The red line is a linear fit through all final Black Silicon structures with sharp tips (full circles) and serves as a guide to the eye.

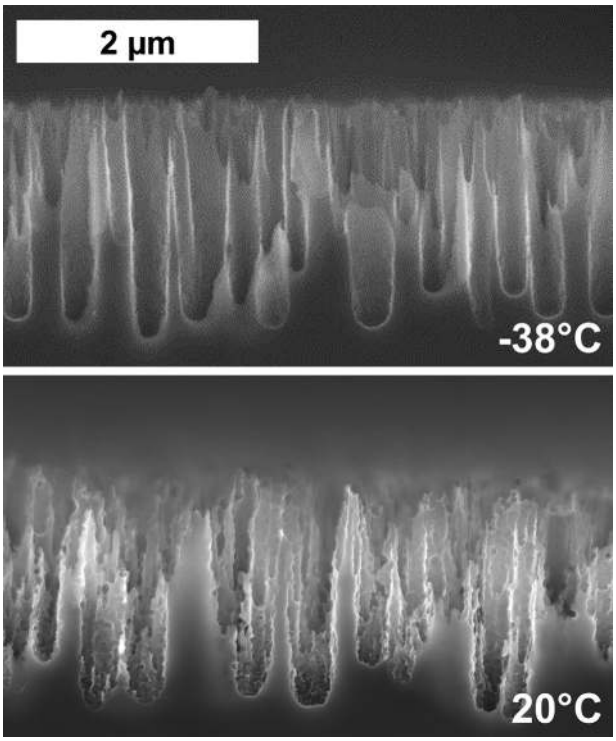


FIG. 14. Cross-section SEM images of Black Silicon established under substrate temperatures of about −38 °C and 20 °C. All other etching parameters are kept constant. The structure correlation lengths at −38 °C and 20 °C amount to 216 nm and 310 nm, respectively.

## V. SUMMARY

The evolution of Black Silicon nanostructures, established by ICP-RIE from the precursor gases $SF_6$ and $O_2$ at non-cryogenic temperatures was discussed comprehensively in this paper. It was shown that structure formation starts from randomly distributed etch pores and continues via pore widening and deepening through silicon etching by fluorine radicals, in which lateral etching is suppressed by the formation of passivating $SiO_xF_y$ at the vertical sidewalls. In course of this process, sharp nanostructure features develop at the intersection points of the growing etch pores that yield a strong suppression of interface reflection and, depending on the mean lateral structure dimensions, a more or less pronounced forward scattering of incident light into higher angles of propagation.

The dependence of nanostructure geometry and the resulting antireflection behavior on the main fabrication parameters etch duration, gas composition and pressure was discussed comprehensively. In particular, a variation of gas composition allows controlling the etching and passivation reactions during structure development, such that structure dimensions can be effectively scaled. The pressure can be used to adjust the isotropy of the etch process and, hence, both the structure dimensions and structure sidewall angles.

The impact of the geometry parameters on the optical properties, namely, antireflection and light trapping effect, was illustrated and explained by means of rigorous optical calculations of numerically synthesized Black Silicon structures. In particular, the non-obvious effect of raising reflectance due to etching in high $SF_6$ plasmas (or at elevated temperatures) could be ascribed unambiguously to the structure sidewall roughness developing under such etching conditions.

Analyzing all Black Silicon nanostructures fabricated by ICP-RIE in our labs so far, a clear trend towards increasing lateral structure dimensions with increasing structure depths was shown that results from the dependence of both structure parameters on the etching reaction in the plasma. This interdependency between lateral and vertical structure dimensions prohibits the creation of Black Silicon with extreme aspect ratios which might be a problem for image preserving, low wavelength applications.

Finally, the applicability of Black Silicon formation by ICP-RIE was discussed. Its ability of being selectively patterned and its producibility at least up to room temperature, as well as recently developed, efficient surface passivation schemes make the fabrication of Black Silicon by ICP-RIE feasible on an industrial scale.

## ACKNOWLEDGMENTS

The authors gratefully acknowledge the financial support by the FO+ (Contract No. 03WKCK1D) and SolarNano (Contract No. 13N13163) funding programs of the German Federal Ministry of Education and Research.

[1]C. Brückner, T. Käsebier, B. Pradarutti, S. Riehemann, G. Notni, E.-B. Kley, and A. Tünnermann, "Broadband antireflective structures applied to high resistive float zone silicon in the THz spectral range," Opt. Exp. **17**(5), 3063–3077 (2009).

[2]C.-H. Sun, P. Jiang, and B. Jiang, "Broadband moth-eye antireflection coatings on silicon," Appl. Phys. Lett. **92**, 061112 (2008).

[3]R. L. Smith and S. D. Collins, "Porous silicon formation mechanisms," J. Appl. Phys. **71**, R1 (1992).

[4]M. Ge, X. Fang, J. Rong, and C. Zhou, "Review of porous silicon preparation and its application for lithium-ion battery anodes," Nanotechnology **24**(42), 422001 (2013).

[5]Y.-F. Huang, S. Chattopadhyay, Y.-J. Jen, C.-Y. Peng, T.-A. Liu, Y.-K. Hsu, C.-L. Pan, H.-C. Lo, C.-H. Hsu, Y.-H. Chang, C.-S. Lee, K.-H. Chen, and L.-C. Chen, "Improved broadband and quasi-omnidirectional anti-reflection properties with biomimetic silicon nanostructures," Nat. Nanotechnol. **2**, 770 (2007).

[6]S. A. Boden and D. M. Bagnall, "Tunable reflection minima of nanostructured antireflective surfaces," Appl. Phys. Lett. **93**, 133108 (2008).

[7]J. Westwater, D. P. Gosain, S. Tomiya, S. Usui, and H. Ruda, "Growth of silicon nanowires via gold/silane vapor-liquid-solid reaction," J. Vac. Sci. Technol. B **15**, 554 (1997).

[8]H. Wang, L. A. Zepeda-Ruiz, G. H. Gilmer, and M. Upmanyu, "Atomistics of vapour-liquid-solid nanowire growth," Nat. Commun. **4**, 1956 (2012).

[9]K. Peng, Y. Yan, S. Gao, and J. Zhu, "Synthesis of large-area silicon nanowire arrays via self-assembling nanoelectrochemistry," Adv. Mater. **14**, 1164–1167 (2002).

[10]Z. Huang, N. Geyer, P. Werner, J. de Boor, and U. Gösele, "Metal-assisted chemical etching of silicon: A review," Adv. Mater. **23**, 285 (2011).

[11]G. Jia, M. Steglich, I. Sill, and F. Falk, "Core–shell heterojunction solar cells on silicon nanowire arrays," Sol. Energy Mater. Sol. Cells **96**, 226–230 (2012).

[12]T.-H. Her, R. J. Finlay, C. Wu, and E. Mazur, "Femtosecond laser-induced formation of spikes on silicon," Appl. Phys. A **70**, 383 (2000).

[13]H. M. Vandriel, J. E. Sipe, and J. F. Young, "Laser-induced coherent modulation of solid and liquid surfaces," J. Luminescence **30**, 446–471 (1985).

[14]H. Jansen, M. de Boer, R. Legtenberg, and M. Elwenspoek, "The black silicon method: A universal method for determining the parameter setting of a fluorine-based reactive ion etcher in deep silicon trench etching with profile control," J. Micromech. Microeng. **5**, 115 (1995).

[15]R. Dussart, X. Mellhaoui, T. Tillocher, P. Lefaucheux, M. Volatier, C. Socquet-Clerc, P. Brault, and P. Ranson, "Silicon columnar microstructures induced by an SF6/O2 plasma," J. Phys. D: Appl. Phys. **38**, 3395–3402 (2005).

[16]J. S. Yoo, I. O. Parm, U. Gangopadhyay, K. Kim, S. K. Dhungel, D. Mangalaraj, and J. Yi, "Black silicon layer formation for application in solar cells," Sol. Energy Mater. Sol. Cells **90**, 3085–3093 (2006).

[17]M. Steglich, T. Käsebier, I. Höger, K. Füchsel, A. Tünnermann, and E.-B. Kley, "Black silicon nanostructures on silicon thin films prepared by reactive ion etching," Chin. Opt. Lett. **11**, S10502 (2013).

[18]J. I. Gittleman, E. K. Sichel, H. W. Lehmann, and R. Widmer, "Textured silicon: A selective absorber for solar thermal conversion," Appl. Phys. Lett. **35**(10), 742–744 (1979).

[19]S. H. Zaidi, D. S. Ruby, and J. M. Gee, "Characterization of random reactive ion etched-textured silicon solar cells," IEEE Trans. Electron Devices **48**(6), 1200–1206 (2001).

[20]J. Pezoldt, T. Kups, M. Stubenrauch, and M. Fischer, "Black luminescent silicon," Phys. Status Solidi C **8**(3), 1021–1026 (2011).

[21]H. V. Jansen, M. J. de Boer, S. Unnikrishnan, M. C. Louwerse, and M. C. Elwenspoek, "Black silicon method X: A review on high speed and selective plasma etching of silicon with profile control: an in-depth comparison between Bosch and cryostat DRIE processes as a roadmap to next generation equipment," J. Micromech. Microeng. **19**, 033001 (2009).

[22]H. V. Jansen, M. J. de Boer, K. Ma, M. Girones, S. Unnikrishnan, M. C. Louwerse, and M. C. Elwenspoek, "Black silicon method XI: Oxygen pulses in SF6 plasma," J. Micromech. Microeng. **20**, 075027 (2010).

[23]A. F. Oskooi, D. Roundy, M. Ibanescu, P. Bermel, J. D. Joannopoulos, and S. G. Johnson, "Meep: A flexible free-software package for electromagnetic simulations by the FDTD method," Comput. Phys. Commun. **181**, 687 (2010).

[24]X. Mellhaoui, R. Dussart, T. Tillocher, P. Lefaucheux, P. Ranson, M. Boufnichel, and L. J. Overzet, "SiOxFy passivation layer in silicon cryoetching," J. Appl. Phys. **98**, 104901 (2005).

[25]T. Tillocher, R. Dussart, X. Mellhaoui, P. Lefaucheux, N. M. Maaza, P. Ranson, M. Boufnichel, and L. J. Overzet, "Oxidation threshold in silicon etching at cryogenic temperatures," J. Vac. Sci. Technol., A **24**, 1073 (2006).

[26]R. Dussart, T. Tillocher, P. Lefaucheux, and M. Boufnichel, "Plasma cryogenic etching of silicon: From the early days to today's advanced technologies," J. Phys. D: Appl. Phys. **47**, 123001 (2014).

[27]H. Jansen, M. de Boer, H. Wensink, B. Kloeck, and M. Elwenspoek, "The black silicon method. VIII. A study of the performance of etching silicon using SF6/O2-based chemistry with cryogenical wafer cooling and a high density ICP source," Microelectron. J. **32**, 769 (2001).
[28]M. Köhler, *Etching in Microsystems Technology* (Wiley-VCH, Weinheim, 1999) pp. 162–163.
[29]E. A. Eklund, R. Bruinsma, J. Rudnick, and R. S. Williams, "Submicron-scale surface roughening induced by ion bombardment," Phys. Rev. Lett. **67**(13), 1759–1762 (1991).
[30]I. Koponen and M. Hautala, "Modeling ion bombardment induced submicron-scale surface roughening," Nucl. Instrum. Methods Phys. Res., Sect. B **103**(2), 156–160 (1995).
[31]M. Boufnichel, P. Lefaucheux, S. Aachboun, R. Dussart, and P. Ranson, "Origin, control and elimination of undercut in silicon deep plasma etching in the cryogenic process," Microelectron. Eng. **77**, 327–336 (2005).
[32]W. H. Southwell, "Pyramid-array surface-relief structures producing anti-reflection index matching on optical surfaces," J. Opt. Soc. Am. A **8**(3), 549–553 (1991).
[33]J. Haynos, J. Allison, R. Arndt, and A. Meulenberg, "The Comsat non-reflective silicon solar cell: a second generation improved cell," in *International Conference on Photovoltaic Power Generation, Hamburg, September, 1974*, p. 487.
[34]T. Yagi, Y. Uraoka, and T. Fuyuki, "Ray-trace simulation of light trapping in silicon solar cell with texture structures," Sol. Energy Mater. Sol. Cells **90**(16), 2647–2656 (2006).
[35]D. A. G. Brüggeman, "Berechnung verschiedener physikalischer Konstanten von heterogenen Substanzen: I. Dielektrizitätskonstanten und Leitfähigkeiten der Mischkörper aus isotropen Substanzen," Ann. Phys. **416**(1–7), 636 (1935).
[36]E. Yablonovitch, "Statistical ray optics," J. Opt. Soc. Am. **72**, 899 (1982).
[37]M. G. Moharam and T. K. Gaylord, "Diffraction analysis of dielectric surface-relief gratings," J. Opt. Soc. Am. **72**, 1385 (1982).
[38]W. H. Southwell, "Gradient-index antireflection coatings," Opt. Lett. **8**, 584 (1983).
[39]S. J. Wilson and M. C. Hutley, "The optical properties of "moth eye" anti-reflection surfaces," Opt. Acta (London) **29**, 993 (1982).
[40]K. Yamamoto, A. Sakamoto, T. Nagano, and K. Fukumitsu, "NIR sensitivity enhancement by laser treatment for Si detectors," Nucl. Instrum. Methods Phys. Res. A **624**, 520–523 (2010).
[41]Z. Li, B. K. Nayak, V. V. Iyengar, D. McIntosh, Q. Zhou, M. C. Gupta, and J. C. Campbell, "Laser-textured silicon photodiode with broadband spectral response," Appl. Opt. **50**(17), 2508–2511 (2011).
[42]Z. Huang, J. E. Carey, M. Liu, X. Guo, E. Mazur, and J. C. Campbell, "Microstructured silicon photodetector," Appl. Phys. Lett. **89**, 033506 (2006).
[43]M. Kroll, M. Otto, T. Käsebier, K. Füchsel, R. Wehrspohn, E.-B. Kley, A. Tünnermann, and T. Pertsch, "Black silicon for solar cell applications," Proc. SPIE **8438**, 843817 (2012).
[44]J. Oh, H.-C. Yuan, and H. M. Branz, "An 18.2%-efficient black-silicon solar cell achieved through control of carrier recombination in nanostructures," Nat. Nanotechnol. **7**, 743–748 (2012).
[45]Y. Inomata, K. Fukui, and K. Shirasawa, "Surface texturing of large area multicrystalline silicon solar cells using reactive ion etching method," Sol. Energy Mater. Sol. Cells **48**, 237 (1997).
[46]Z. Shen, B. Liu, Y. Xia, J. Liu, J. Liu, S. Zhong, and C. Li, "Black silicon on emitter diminishes the lateral electric field and enhances the blue response of a solar cell by optimizing depletion region uniformity," Scr. Mater. **68**, 199 (2013).
[47]M. Steglich, D. Lehr, S. Ratzsch, T. Käsebier, F. Schrempel, E.-B. Kley, and A. Tünnermann, "An ultra-black silicon absorber," Laser Photonics Rev. **8**(2), L13–L17 (2014).
[48]S. Kalem, P. Werner, Ö. Arthursson, V. Talalaev, B. Nilsson, M. Hagberg, H. Frederiksen, and U. Södervall, "Black silicon with high density and high aspect ratio nanowhiskers," Nanotechnology **22**, 235307 (2011).
[49]H. Jansen, H. Gardeniers, M. de Boer, M. Elwenspoek, and J. Fluitman, "A survey on the reactive ion etching of silicon in microtechnology," J. Micromech. Microeng. **6**, 14–28 (1996).
[50]K. N. Nguyen, P. Basset, F. Marty, Y. Leprince-Wang, and T. Bourouina, "On the optical and morphological properties of microstructured Black Silicon by cryogenic-enhanced plasma reactive ion etching," J. Appl. Phys. **113**, 194903 (2013).
[51]D. Murias, C. Reyes-Betanzo, M. Moreno, A. Torres, A. Itzmoyotl, R. Ambrosio, M. Soriano, J. Lucas, and P. Roca i Cabarrocas, "Black Silicon formation using dry etching for solar cell applications," Mater. Sci. Eng. B **177**, 1509–1513 (2012).
[52]M. Ernst, R. Brendel, R. Ferré, and N.-P. Harder, "Thin macroporous silicon heterojunction solar cells," Phys. Status Solidi **6**, 187 (2012).
[53]K. Peng, Y. Xu, Y. Wu, Y. Yan, S.-T. Lee, and J. Zhu, "Aligned single-crystalline Si nanowire arrays for photovoltaic applications," Small **1**, 1062 (2005).
[54]E. C. Garnett and P. Yang, "Silicon nanowire radial p-n junction solar cells," J. Am. Chem. Soc. **130**, 9224 (2008).
[55]M. Otto, M. Kroll, T. Käsebier, R. Salzer, A. Tünnermann, and R. B. Wehrspohn, "Extremely low surface recombination velocities in black silicon passivated by atomic layer deposition," Appl. Phys. Lett. **100**, 191603 (2012).